Available online at www.sciencedirect.com

SciVerse ScienceDirect

Journal of the European Ceramic Society 32 (2012) 1743–1749

www.elsevier.com/locate/jeurceramsoc

R-curve behavior, mechanical properties and microstructure of sintered ZrB_2–SiC_p–ZrO_{2f} ceramics

Lin Jia [a,*], Zhang Xinghong [a], Cao Huijun [b], Jin Hua [a], Han Wenbo [a]

[a] *National Key Laboratory of Science and Technology on Advanced Composites in Special Environments, Harbin Institute of Technology, Harbin 150001, China*
[b] *Shenzhen Graduate School, Harbin Institute of Technology, Shenzhen 518055, China*

Received 7 December 2011; received in revised form 22 January 2012; accepted 25 January 2012
Available online 17 February 2012

Abstract

In this paper, zirconium diboride based ceramics added with 20 vol.% silicon carbide particle and 15 vol.% zirconia fiber ($Z20S_p15Z_f$) were prepared by hot-pressing at 1850 °C for 60 min under a uniaxial load of 30 MPa in Ar atmosphere. *R*-curves for $Z20S_p15Z_f$ ceramics were studied using the indentation-strength in bending technique and the envelope method. The results indicated that these two testing methods were consistent and viable for estimating *R*-curve. $Z20S_p15Z_f$ ceramics had high resistance to crack growth and damage tolerance with the 6.8 MPa m$^{1/2}$ of steady-state toughness. The toughening mechanism was fiber debonding, fiber pull-out, crack bridging, crack branching, crack deflection and transformation toughening.

Keywords: A. Hot pressing; B. Fibers; C. Fracture; E. Structural applications

1. Introduction

The traditional ceramics exhibit a large strength scatter because of the poor crack tolerance and the wide range of flaws induced by fabrication and machining processes.[1] Recent studies have proved that the improvement in the strength reliability comes from the crack resistance curve (*R*-curve).[2,3] *R*-curve behavior of ceramics has attracted wide attention in the past decades, which describes the increase in crack growth resistance during stable crack extension before instability and can be expressed by a power-law equation[1]:

$$K_R = A(\Delta c)^n \tag{1}$$

where K_R is the crack resistance, A and n are material constants, Δc is the increase in crack length, $\Delta c = c - c_0$, c_0 is a preexisting, traction-free notch. The exponent n measures susceptibility to *R*-curve behavior. A rising *R*-curve denotes that additional energy is required not only to meet the need at the crack tip to propagate the crack, but also to overcome extrinsic toughening mechanisms, such as crack bridging and crack deflection.[4,5] *R*-curve is now known to have a profound influence on the mechanical properties of ceramics, such as fracture toughness, cycle fatigue and thermal shock behavior.[6] In order to predict the instability of ceramics, characterizing and understanding *R*-curve behavior are of great importance. According to the numerical calculation and experimental progress in the literature, the testing methods of estimating *R*-curve are summarized.[7–10] One is direct method, including indentation method, single-edge notched beam test and double cantilever beam method. For all these methods, the crack length must be measured and the corresponding stress states are recorded, respectively. However, it is difficult to determine the crack position and monitor stable crack growth. The other is indirect method without direct measuring of crack length, such as the envelope method. Compared with the conventional testing methods, the indirect method provides a unique simplicity and economy in test procedure, at little cost in reliability.

As one of the ultra-high temperature ceramics (UHTC), zirconium diboride (ZrB_2) has the lowest theoretical density (6.09 g cm^{-3}), which makes it attractive for aerospace applications.[11] Furthermore, ZrB_2 has excellent properties such as high melting point (>3000 °C), high thermal and electrical conductivities, chemical inertness against molten metals and great thermal shock resistance, so that it is a potential candidate

* Corresponding author. Tel.: +86 451 86402382; fax: +86 451 86402382.
E-mail address: jiajia10182003@hit.edu.cn (J. Lin).

0955-2219/$ – see front matter © 2012 Elsevier Ltd. All rights reserved.
doi:10.1016/j.jeurceramsoc.2012.01.028

material for high-temperature structural application, including hypersonic aircraft, furnace elements, plasma-arc electrodes, reusable launch vehicles, or rocket engines and thermal protection structures for leading edge parts on hypersonic reentry space vehicles at over 1800 °C.[12,13] However, because of strong covalent bonding and low self-diffusion, monolithic ZrB_2 is difficult to get densified without high temperatures and external pressures. Moreover, the intrinsic brittleness leads to catastrophic failure and poor thermal shock resistance of ZrB_2-based ceramics, which also limits their practical applications. Our previous work[14,15] has confirmed that the addition of silicon carbide particle (SiC_p) and zirconia fiber (ZrO_{2f}) to the ZrB_2 matrix results in the improvement in both densification process and fracture toughness. The toughening mechanism with lack of researching in the ternary ZrB_2–SiC_p–ZrO_{2f} ceramics is complex.

The previous work proved that ZrB_2 added with 20 vol.% SiC_p and 15 vol.% ZrO_{2f} ($Z20S_p15Z_f$) had optimal flexural strength and fracture toughness.[14] In the present study, $Z20S_p15Z_f$ ceramics were fabricated by hot-pressing. The phase composition and microstructure of the $Z20S_p15Z_f$ ceramics were investigated. The damage resistance and *R*-curves behavior of the $Z20S_p15Z_f$ ceramics were evaluated by using the indentation-strength in bending (ISB) technique, and compared with the envelope method, the difference between the two being analyzed.

2. Experimental procedures

2.1. Preparation

Commercially available ZrB_2 powder (2 μm, purity > 99.5%, Northwest Institute for Non-ferrous Metal Research, China) and SiC (1 μm, purity > 99.5%, Weifang Kaihua Micro-powder Co., Ltd., China) were used as raw material. The ZrO_2 fiber (mean diameter and length are 5–8 μm and 200 μm, respectively, purity > 99%, Shandong Huolong Ceramic Fiber Co., Ltd., China) used here was 3 mol.% Y_2O_3 partially stabilized zirconia. The powders were weighed in proportion to the stoichiometric ratio to yield ZrB_2–20 vol.%SiC_p–15 vol.%ZrO_{2f} and then ball-mixed for 20 h in a polyethylene bottle using zirconia balls and ethanol as the grinding media. After mixing, the slurry was dried in a rotary evaporator. The resulting powders were crushed and then passed through a 100-mesh sieve. The resulting powder mixtures were hot-pressed at 1850 °C for 60 min under a uniaxial load of 30 MPa in Ar atmosphere.

2.2. Characterization

The phase composition was determined by X-ray diffraction (XRD; Rigaku, Dmax-rb, CuKa = 1.5418 Å). According to the formula of Toraya et al., the volume fraction of the *m*-ZrO_2 (V_m) was calculated by measuring the intensities of (111) and $(11\bar{1})$ reflections of the monoclinic phase and the (111) peak of the tetragonal phase[16]:

$$V_m = \frac{1.311X_m}{1 + 0.311X_m} \tag{2}$$

$$X_m = \frac{I_m(111) + I_m(11\bar{1})}{I_m(111) + I_m(11\bar{1}) + I_t(111)} \tag{3}$$

where X_m denoted the integrated intensity ratio, I_m and I_t were the peak intensities of the *m*-ZrO_2 and *t*-ZrO_2, respectively. Furthermore, the obtained V_m was individually normalized to the volume fraction of ZrO_2 (V_{ZrO_2}) in each composite as follows:

$$V_{mtot} = V_m \times V_{ZrO_2} \times 100\% \tag{4}$$

Therefore, the result of V_{mtot} on the fracture surface minus the one on the polished surface equals to the transformation fraction from *t*-ZrO_2 to *m*-ZrO_2 during fracture (i.e., *t*-ZrO_2 transformability).

The microstructural features and fragmented surfaces of the hot-pressed ceramic were observed by scanning electron microscopy (SEM, FEI Sirion, Holland). Flexural strength (σ) was tested in three-point bending on 3 mm by 4 mm by 36 mm bars, using a 30 mm span and a crosshead speed of 0.5 mm min^{-1}. Each specimen was ground and polished with diamond slurries down to a 1 μm finish. The edges of all the specimens were chamfered to minimize the effect of stress concentration due to machining flaws. Young's modulus (*E*) was evaluated from the slopes of load deflection curves of above strength tests. A static extensometer was used to measure the deflection with an error in the measurement of 0.1%.

For crack-growth experiments, Vickers' indentation under applied loads between 4.9 and 147 N for 10 s was made at the center of the prospective tensile surface of each test piece. After the indentation test, the indentation strength of specimens was performed immediately by three-points bending tests after indentation in order to avoid any subcritical crack growth due to the stress corrosion effect. The indentation strengths were determined from the failure load as above strength test. At least six specimens were tested for each experimental condition.

2.3. Determination of R-curve

The indentation cracks are used to estimate the toughness of brittle ceramics. During post-indentation bending, the crack is subjected to a total stress intensity factor, K_I, as shown in Eq. (5) [17]:

$$K_I = K_\sigma + K_r + K_s \tag{5}$$

where K_σ, K_r and K_s are the bending stress intensity factor, the indentation residual stress intensity factors and the residual surface stress intensity factors, respectively. In this study, the residual surface stress generated by machine grinding can be eliminated completely by appropriate annealing process, $K_s = 0$. So Eq. (5) can be normalized to

$$K_I = K_\sigma + K_r = \psi\sigma c^{1/2} + \chi P c^{-3/2} \tag{6}$$

where σ, P and c are the applied stress, the indentation load and the crack length, respectively. Parameter ψ is a shape factor of crack geometry, which is treated as a constant (∼1.24) in the evaluation of fracture toughness or *R*-curve behavior of ceramics

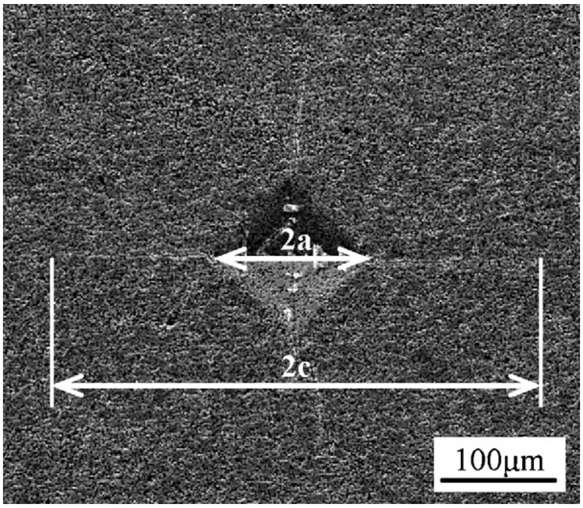

Fig. 1. SEM image of Vickers' indentation (taken at 147 N) on the polished surface of $Z20S_p15Z_f$ ceramics.

using indentation cracks. This hypothesis is valid based on the crack size is much smaller than the bend specimen dimensions and the crack shape is semicircular and invariant during stable crack extension. The indenter geometry-material constant χ is defined as

$$\chi = \delta\left(\frac{E}{H}\right)^{1/2} \tag{7}$$

where E and H are Young's modulus and the hardness of the material, respectively. Parameter δ is a non-dimensional constant that depends on the indenter geometry and Poisson's ratio of the material, and according to the research of Anstis et al.,[18] it can be assumed to be constant, $\delta = 0.016 \pm 0.004$.

According to the energy principle, the crack will grow if applied K_I is equal to or greater than the fracture resistance of the material, K_R. An equilibrium position will be attained at $K_I = K_R$ if the condition of $\mathrm{d}K_I/\mathrm{d}c < \mathrm{d}K_R/\mathrm{d}c$ is satisfied. For a given indentation load P and the corresponding applied stress $\sigma = \sigma_f$, the criterion for the onset of crack-extension instability, leading finally to rupture, is the common-tangent intersection for the K_I and K_R curves,

$$K_I = K_R \tag{8}$$

$$\frac{\mathrm{d}K_I}{\mathrm{d}c} = \frac{\mathrm{d}K_R}{\mathrm{d}c} \tag{9}$$

For the envelope method, according to Eq. (6), the families of $K_I(c)$ curves can be generated from the (σ_f, P) data sets. Then, based on the assumption of Eqs. (8) and (9), $K_R(c)$ curve can be calculated objectively as the envelopes of tangency points to these families of $K_I(c)$ curves using the program of Matlab, so the R-curve is produced.

For the ISB method, the crack length is measured using scanning electron microscopy, as shown in Fig. 1. The $K_R(c)$ curve is estimated by solving Eqs. (6) and (8). In other word, the R-curve can be determined from the (c, σ_f, P) data sets.

3. Results and discussion

3.1. Indentation load and strength

According to the reported work,[4] Griffith materials, which show no rising behavior, would follow the power law:

$$\sigma_f \propto P^{-\beta} \tag{10}$$

where $\beta = 1/3$. On the contrary, materials with slopes less than 1/3 would have R-curve behavior. After taking logarithm of Eq. (10), the relationship between fracture strength σ_f and indentation load P can be expressed as follows:

$$\log\ \sigma_f \propto -\beta \log P \tag{11}$$

Li et al. reported that ZrB_2 added with 10 vol.% silicon carbide particle (SiC_p) and 10 vol.% zirconia particle (ZrO_{2p}) ($Z10S_p10Z_p$) had the most excellent combination of mechanical properties and thermal shock behavior.[19,20] Fig. 2 plots the logarithm of observed bending strength versus the logarithm of indentation load for the $Z20S_p15Z_f$ ceramics, compared with that for monolithic ZrB_2 and $Z10S_p10Z_p$ which are collected from the published literature.[21] Linear regression was applied to calculate the best fit to the data. As shown in Fig. 2, in the high-indentation-load region, the fracture strength of three materials reduced linearly with the increasing indentation load. The slope decreased from 0.341 for monolithic ZrB_2 to 0.231 for $Z10S_p10Z_p$ and 0.181 for $Z20S_p15Z_f$. According to the judgment criterion of Griffith materials, monolithic ZrB_2 is expected to show no rising R-curve behavior, but the $Z10S_p10Z_p$ and $Z20S_p15Z_f$ ceramics with slopes lower than 1/3 are expected to have rising R-curve behavior. Moreover, the flexural strength after indentation varied less rapidly with indentation load for $Z20S_p15Z_f$ than the one for monolithic ZrB_2 and $Z10S_p10Z_p$. This result indicated that the $Z20S_p15Z_f$ ceramics had improved damage resistance in comparison with the monolithic ZrB_2 and $Z10S_p10Z_p$ ceramics. In other words, it was implied that the $Z20S_p15Z_f$ ceramics would have higher rising R-curve behavior than that of the monolithic ZrB_2 and $Z10S_p10Z_p$ ceramics.

3.2. R-curves (the envelope method)

Fig. 3 shows the families of $K_I(c)$ curves and the envelopes of tangency points for the $Z20S_p15Z_f$ ceramic. It could be seen from Fig. 3, the envelope curve of tangency points, which was fitted by using the program of Matlab, formed the rising R-curve behavior. This result indicated that the fracture toughness of the $Z20S_p15Z_f$ ceramics increased with the increase of crack length.

3.3. R-curves (the ISB method)

The scattered points of fracture toughness data obtained by the ISB method are plotted in Fig. 4a, which agree well with the heavy line obtained by the envelope method, also exhibit the typical R-curve behavior. The result proved that these two testing methods were consistent and feasible for estimating R-curve,

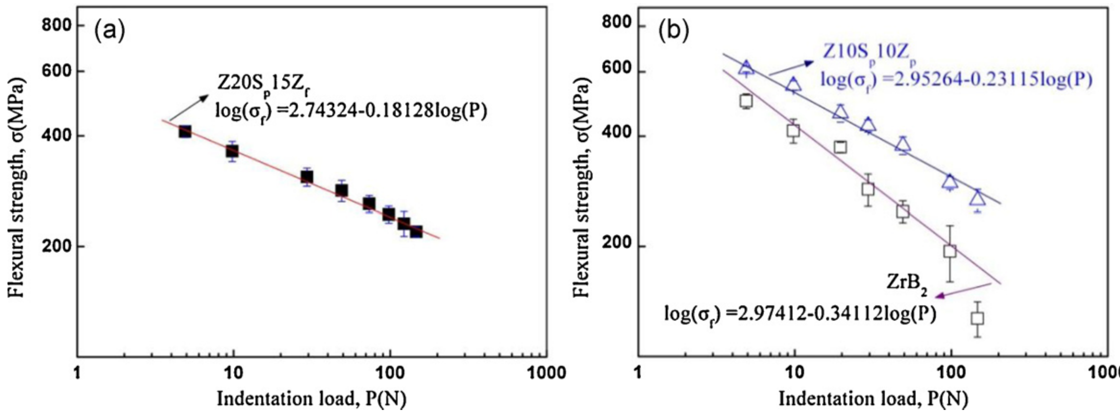

Fig. 2. Strength response to indentation load for (a) $Z20S_p15Z_f$ and (b) ZrB_2, $Z10S_p10Z_p$[21] ceramics.

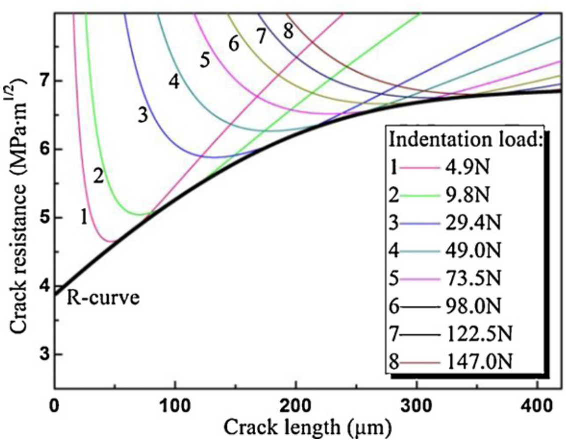

Fig. 3. *R*-curve for $Z20S_p15Z_f$ ceramics (the envelope method).

and accurate data acquisition was achieved. Fig. 4b displays that fracture toughness is plotted as a function of crack length for ZrB_2 and $Z10S_p10Z_p$ ceramics, respectively, which are collected from the published literature.[21] Obviously, monolithic ZrB_2 showed a plateau *R*-curve behavior, which was almost horizontal. The slope of 0.341 in Fig. 2b, close to 1/3, also confirmed the soft *R*-curve behavior for monolithic ZrB_2, which could be mainly attributed to the absence of extrinsic toughening mechanisms.[21] Compared with monolithic ZrB_2, $Z10S_p10Z_p$ ceramics provided obvious *R*-curve, and the value of steady-state toughness was ~6.4 MPa m$^{1/2}$, which was contributed to the interaction of transformation toughening and crack bridging. Evidently, as shown in Fig. 4a, the present $Z20S_p15Z_f$ ceramics had higher rising *R*-curve behavior. $Z20S_p15Z_f$ ceramics had an initial toughness in the short crack region (<100 μm) higher than both monolithic ZrB_2 and $Z10S_p10Z_p$ ceramics. The crack growth propagated continuously, *R*-curve behavior became stronger so that the stress intensity factor, which was required to promote stable crack growth, increased rapidly until the steady-state toughness was obtained. In the case of $Z20S_p15Z_f$ ceramics, the value of steady-state toughness was ~6.8 MPa m$^{1/2}$. This suggested that $Z20S_p15Z_f$ ceramic possessed excellent damage tolerance and a rising *R*-curve behavior in comparison with both monolithic ZrB_2 and $Z10S_p10Z_p$ ceramics.

3.4. The toughening mechanism

Fig. 5 is the typical SEM micrographs of the fracture surface of the $Z20S_p15Z_f$ ceramics. As seen from the insert magnification in Fig. 5B, the perfect interface between zirconia fiber and other phases was displayed, which was favorable to fiber debonding and pull-out. The fiber debonding, pull-out and

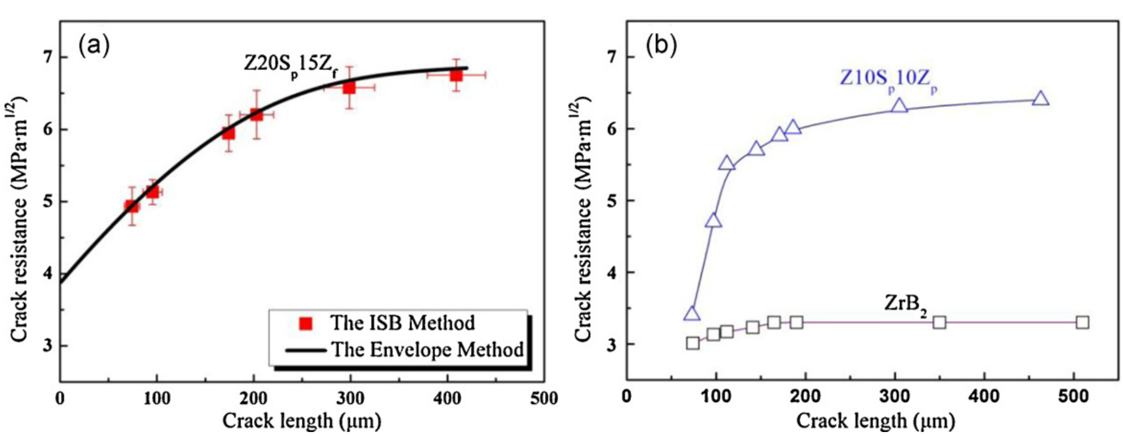

Fig. 4. *R*-curve behavior for (a) $Z20S_p15Z_f$ (the ISB method) and (b) ZrB_2, $Z10S_p10Z_p$[21] ceramics.

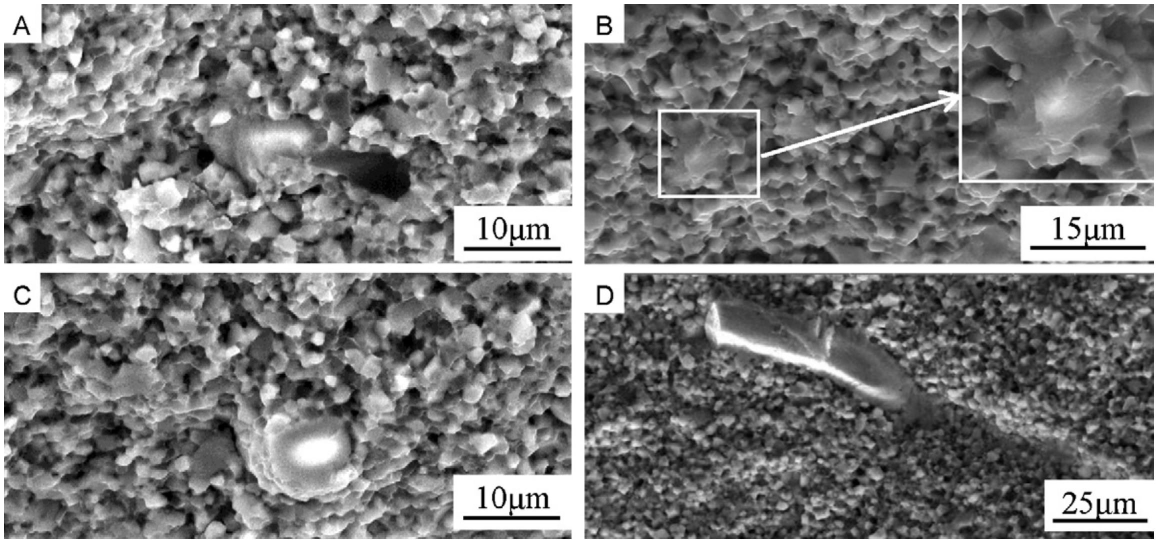

Fig. 5. Fracture surfaces of $Z20S_p15Z_f$ ceramics.

fracture were observed on the rough fractured surface, which indicated that the stress intensity factor at the crack tip overcame not only the crack growth resistance of matrix, but also the interfacial shear resistance. The debonding, pull-out and fracture fiber would improve the fracture toughness of the ceramics.

The SEM micrographs of cracks path obtained by the indentation on the polished surface of the $Z20S_p15Z_f$ ceramics are shown in Fig. 6. The tortuous crack propagation path indicated that crack deflection occurred along weak interface might be another toughening mechanism since the crack swerving and

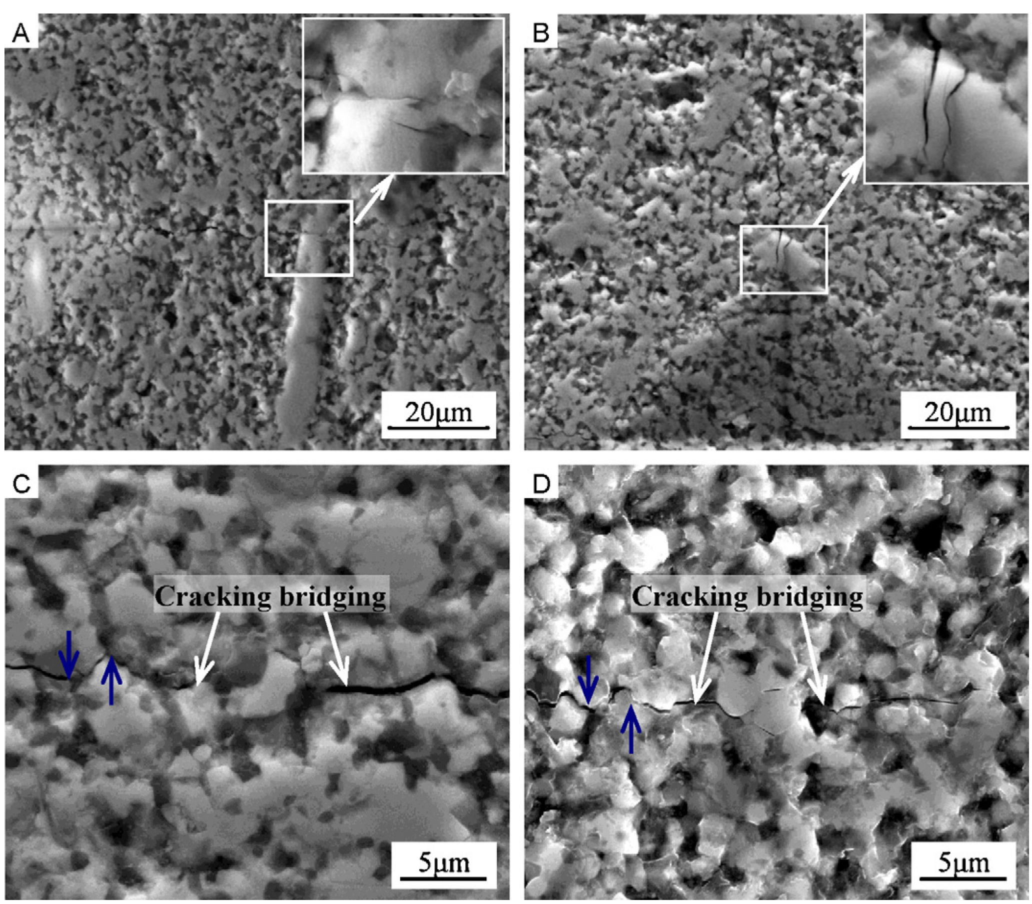

Fig. 6. Typical crack propagation on the polished surface of the $Z20S_p15Z_f$ ceramics.

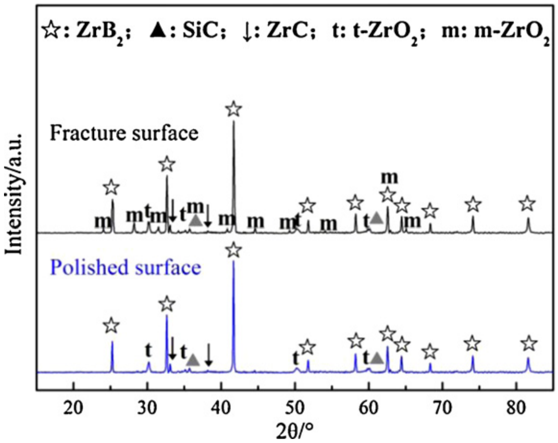

Fig. 7. XRD spectra obtained from the fracture surface and polished surface of the $Z20S_p15Z_f$ ceramics.

twisting along fiber/matrix interface exhausted more energy than crack propagating straightforward.[4] In addition, the obvious crack branching and bridging were displayed. In general, the crack path was deflected and branched along the weak interface in the matrix. The pulled-out fibers had bridging effects on crack propagation behind crack tip. The crack path became devious and the work of fracture (WOF) increased. Hence, the fracture toughness of the $Z20S_p15Z_f$ ceramics increased as the crack length increased. Undoubtedly, such integrated toughening effect consumed the energy of crack propagation during fracturing process and led to the improvement of the fracture toughness.

Besides the above toughening mechanisms, phase transformation toughening is another important contribution to toughen zirconia-containing composites.[21] An XRD spectra obtained from the fractured and polished surface of the $Z20S_p15Z_f$ ceramics are shown in Fig. 7. Apparently, the phase analysis indicated the main phases in the polished surface of the $Z20S_p15Z_f$ ceramics were ZrB_2, SiC and t-ZrO_2 as well as a trace of ZrC, which was attributed to the reaction of silicon carbide particle and zirconia fiber. As seen in Fig. 7, the diffraction peak of m-ZrO_2 phase was observed in the fractured surface of the $Z20S_p15Z_f$ ceramics. According to Eqs. (2)–(4), t-ZrO_2 transformability during fracturing process can be calculated. As known, when subjected to the external load, stress concentration in the hot-pressed $Z20S_p15Z_f$ ceramics will bring the phase transformation from t-ZrO_2 to m-ZrO_2 with volume change,[22] which will restrain the crack growing or propagating and exhaust the fracture energy. Resultantly, the combination effects of all these toughening mechanisms above provide a valuable way to toughen ZrB_2-based ceramics.

4. Conclusions

The $Z20S_p15Z_f$ ceramics were fabricated by hot-pressing at 1850 °C for 60 min under a uniaxial load of 30 MPa in Ar atmosphere. The experimental results and analysis of the crack growth resistance behavior of $Z20S_p15Z_f$ were studied using the indentation-strength in bending technique with a comparison of the envelope method. The results proved that these two testing methods were uniform and viable for estimating R-curve. Under three-points bending tests, the crack growth resistance property of $Z20S_p15Z_f$ ceramics exhibited rising R-curve behavior, and the toughness reached a steady-state value at 6.8 MPa m$^{1/2}$. Such improvements in damage tolerance and R-curve behavior were due to the toughening mechanism, such as fiber debonding, fiber pull-out, crack branching, crack bridging, crack deflection and transformation toughening.

Acknowledgments

This work was supported by the NSFC (51072042, 10725207) and the Science Fund for Outstanding Youths of Heilongjiang Province.

References

1. Duan K, Mai YW, Cotterell B. R-curve effect on strength and reliability of toughened ceramic materials. *J Mater Sci* 1995;**30**:1405–8.
2. Tomaszewski H, Boniecki M, Weglarz H. Effect of grain size on R-curve behaviour of alumina ceramics. *J Eur Ceram Soc* 2000;**20**:2569–74.
3. Linda MB, Stephen JB, Brian RL. Objective evaluation of short-crack toughness curves using indentation flaws: case study on alumina-based ceramics. *J Am Ceram Soc* 1992;**75**:3049–57.
4. Kim YW, Mitomo M. R-curve behaviour and microstructure of sintered silicon nitride. *J Mater Sci* 1995;**30**:5178–84.
5. Robb MK, Fengchun J, Kenneth SV. Loading rate effects on the R-curve behavior of cortical bone. *Acta Biomater* 2011;**7**:724–32.
6. Ameli A, Papini M, Schroeder JA, Spelt JK. Fracture R-curve characterization of toughened epoxy adhesives. *Eng Fract Mech* 2010;**77**: 521–34.
7. Jiang T, Jin ZH, Yang JF, Qiao GJ. Mechanical property and R-curve behavior of the B_4C/BN ceramics composites. *Mater Sci Eng A* 2008;**494**: 203–16.
8. Li CW, Lee DJ, Lui SC. R-curve behavior and strength for in situ reinforced silicon nitrides with different microstructures. *J Am Ceram Soc* 1992;**75**:1777–85.
9. Robert FC, Brian RL, Carolyn JF. Microstructure-strength properties in ceramics. I. Effect of crack size on toughness. *J Am Ceram Soc* 1985;**68**:604–15.
10. Keisuke T, Yoshiaki A, Hirohisa K, Yasuki K. R-curve behavior in fracture of notched porous ceramics. *Eng Fract Mech* 2003;**70**:1101–13.
11. Ipek A, Mikinori H, Filiz CS, Onuralp Y, Gultekin G, Takashi G. Microstructure and densification of ZrB_2–SiC composites prepared by spark plasma sintering. *J Eur Ceram Soc* 2009;**29**:2379–85.
12. Brochu M, Gauntt BD, Boyer L, Loehman RE. Pressureless reactive sintering of ZrB_2 ceramic. *J Eur Ceram Soc* 2009;**29**:1493–9.
13. Lingappa R, Canchi D, Vikram J. Fabrication and mechanisms of densification of ZrB_2-based ultra high temperature ceramics by reactive hot pressing. *J Eur Ceram Soc* 2010;**30**:129–38.
14. Lin J, Zhang XH, Wang Z, Han WB. Microstructure and mechanical properties of ZrB_2–SiC–ZrO_{2f} ceramic. *Scripta Mater* 2011;**64**:872–5.
15. Lin J, Zhang XH, Wang Z, Han WB, Jin H. Microstructure and mechanical properties of hot-pressed ZrB_2–SiC–ZrO_{2f} ceramics with different sintering temperatures. *Mater Des* 2012;**34**:853–6.
16. Toraya H, Yoshimura M, Somiya S. Calibration curve for quantitative analysis of the monoclinic-tetragonal ZrO_2 System by X-ray diffraction. *J Am Ceram Soc* 1984;**67**:119–21.
17. Ralph Jr FK. Rising fracture toughness from the bending alumina beams. *J Am Ceram Soc* 1988;**71**:338–43.
18. Anstis GR, Chantikul P, Lawn BR, Marshall DB. A critical evaluation of indentation techniques for measuring fracture toughness. I. Direct crack measurements. *J Am Ceram Soc* 1981;**64**:533–8.

19. Zhang XH, Li WJ, Hong CQ, Han WB, Han JC. Microstructure and mechanical properties of hot pressed ZrB_2–SiC_p–ZrO_2 composites. *Mater Lett* 2008;**62**:2404–6.
20. Chen DJ, Li WJ, Zhang XH, Hu P, Han JC, Hong CQ, et al. Microstructural feature and thermal shock behavior of hot-pressed ZrB_2–SiC–ZrO_2 composite. *Mater Chem Phys* 2009;**116**: 348–52.
21. Zhu T, Li WJ, Zhang XH, Hu P, Hong CQ, Weng L. Damage tolerance and R-curve behavior of ZrB_2–ZrO_2 composites. *Mater Sci Eng A* 2009;**516**:297–301.
22. Zhao HL, Li X, Ju F, Pal U. Effects of particle size of 8 mol% Y_2O_3 stabilized ZrO_2(YSZ) and additive Ta_2O_5 on the phase composition and the microstructure of sintered YSZ electrolyte. *J Mater Process Technol* 2008;**200**:199–204.